Electron-vibrational coupling in the Fenna-Matthews-Olson complex of Prosthecochloris aestuarii determined by temperature dependent absorption and fluorescence line narrowing measurements

Wendling, M.; Pullerits, T.; Przyjalgowski, M.A.; Vulto, S.I.E.; Aartsma, T.J.; van Grondelle, R.; van Amerongen, H.

published in
Journal of Physical Chemistry B
2000

DOI (link to publisher)
10.1021/jp000077+

document version
Publisher's PDF, also known as Version of record

Electron−Vibrational Coupling in the Fenna−Matthews−Olson Complex of *Prosthecochloris aestuarii* Determined by Temperature-Dependent Absorption and Fluorescence Line-Narrowing Measurements

Markus Wendling,*,† Tõnu Pullerits,‡ Milosz A. Przyjalgowski,† Simone I. E. Vulto,§,|| Thijs J. Aartsma,§ Rienk van Grondelle,† and Herbert van Amerongen†

Vrije Universiteit, Faculty of Sciences, Division of Physics and Astronomy, Department of Biophysics and Physics of Complex Systems, De Boelelaan 1081, 1081 HV Amsterdam, The Netherlands, Lund University, Department of Chemical Physics, Box 124, 22100 Lund, Sweden, and Rijksuniversiteit Leiden, Department of Biophysics, Huygens Laboratory, P.O. Box 9504, 2300 RA Leiden, The Netherlands

Received: January 6, 2000; In Final Form: March 6, 2000

Fluorescence line-narrowing measurements at low temperature were performed on the Fenna−Matthews−Olson complex of *Prosthecochloris aestuarii*. Superimposed on the phonon wing, several vibronic bands could be observed. By use of these data, the temperature dependence of the lowest-energy absorption band was modeled based on the linear harmonic Franck−Condon approximation. The overall Huang−Rhys factor was estimated to be 0.45. The maximum of the phonon distribution was located at 20 cm^{-1}. Thirty vibrational modes could be observed, and their Franck−Condon factors were estimated. The strongest modes were located at 36, 70, and ∼195 cm^{-1}. For the full width at half-maximum of the inhomogeneous broadening, a value of 80 cm^{-1} was determined. We did not find any evidence for the presence of different excitonic states in the lowest-energy absorption band.

Introduction

Photosynthesis is the synthesis of organic compounds by the use of photons: the energy of sunlight is converted into chemical energy. The primary steps in this process are "light harvesting" and charge separation. For light harvesting, all photosynthetic organisms have so-called antenna complexes. The function of these pigment−protein complexes is to absorb light and to transport the excited-state energy finally to a special pigment−protein complex—the photosynthetic reaction center (RC), where charge separation occurs.[1,2]

The green sulfur bacteria have two kinds of antenna complexes. In addition to the chlorosomes is found a bacteriochlorophyll (BChl) *a* containing protein, commonly referred to as the Fenna−Matthews−Olson (FMO) complex. Aggregates of FMO connect the chlorosomes and the photosynthetic membrane that hosts the RC.[3]

The FMO complex of the green sulfur bacterium *Prosthecochloris (Pc.) aestuarii* was the first photosynthetic protein for which the crystal structure was determined.[4] It is now known at a resolution of 1.9 Å.[5,6] FMO occurs as a trimer, and each of the monomers consists of a protein folded as a "string bag". The FMO monomer binds seven BChl *a* molecules. The average center-to-center distance between nearest-neighbor pigments within a monomer unit is 12 Å. The closest distance between pigments in adjacent subunits is 24 Å.[3]

The detailed knowledge of its crystallographic structure makes the FMO complex a highly suitable model system for theoretical and experimental studies aimed at unravelling the relationship between structure and spectroscopy in the FMO complex. In particular, excitonic modeling of the low-temperature steady-state spectra has been performed. Early attempts to fit simultaneously low-temperature absorption and circular dichroism (CD) spectra considering only a monomer were not very successful.[7] When the coupling between pigments in different subunits of the trimer was also included, the agreement between calculations and experiments was improved substantially.[8] A simultaneous simulation of the absorption, linear dichroism (LD), and triplet-minus-singlet (T−S) absorption difference spectra by Gülen also relied on the trimeric structure.[9] Interestingly, in a spectral hole-burning study by Johnson and Small on the FMO complex of *Pc. aestuarii*,[10] a satellite hole of the lowest-energy band at 825 nm at low temperature was observed, which was interpreted as an additional excitonic component due to the interaction of BChl *a* molecules in different subunits within a trimer. Rätsep et al.[11] found three lowest-energy Q_y states in the 825 nm band of the FMO complex of *Chlorobium tepidum* by hole burning, which were explained by structural heterogeneity leading to a different energy of the lowest excited state in each subunit of the trimer. Whereas the satellite hole in ref 10 was thought to be due to an excitonic state delocalized over the trimer, the three lowest-energy states in ref 11 were all thought to be localized in monomeric subunits. From the polarization properties of the T−S absorption difference spectrum of the FMO complex of *Pc. aestuarii*, van Mourik et al.[12] concluded that the 825 nm band consists of three exciton components: two degenerate transitions that completely determine the 825 nm absorption band and one slightly red-shifted transition with a negligibly small contribution to the absorption spectrum.

* Author to whom correspondence should be addressed. Markus Wendling, Vrije Universiteit, Faculty of Sciences, Division of Physics and Astronomy, Department of Biophysics and Physics of Complex Systems, De Boelelaan 1081, 1081 HV Amsterdam, The Netherlands. Telephone: +31-20-4447932. Fax: +31-20-4447899. E-mail: markus@nat.vu.nl.

† Vrije Universiteit.

‡ Lund University.

§ Rijksuniversiteit Leiden.

|| Present address: Philips Research Laboratories, Building WB6, Prof. Holstlaan 4, 5656 AA Eindhoven, The Netherlands.

10.1021/jp000077+ CCC: $19.00
Published on Web 05/26/2000

Louwe et al.[13] have recently achieved remarkably good agreement between experimental and calculated steady-state spectra of the FMO complex considering only the monomeric subunit. Not only the absorption and CD spectra, but also the LD, T−S, and linear-dichroic T−S spectra were fit quite well. Despite the relative simplicity of the model, the simulations fit the experimental results better than previous attempts.

In none of the above calculations was the coupling of the electronic and nuclear degrees of freedom (electron−vibrational coupling) considered. At the same time, electron−vibrational coupling is a key for understanding relaxation processes in electronic systems, including the functioning of the FMO complex in excitation transfer among the BChl molecules within the FMO monomers, between monomers, and as a link between chlorosomes and the RC. Recently, Renger and May have studied exciton relaxation in the FMO complex of *Chlorobium tepidum* by applying Redfield relaxation theory.[14] The authors used three different generic functions to describe the weighted frequency spectrum of nuclear modes (spectral density). Clearly, for a more in-depth analysis, knowledge of the spectral densities from an independent experiment would be desirable. In the current work, we address this issue.

There are two types of electron−vibrational coupling: vibronic coupling, i.e., coupling of the electronic transition to intramolecular modes of the chromophore, and electron−phonon coupling, i.e., coupling to intermolecular vibrations of the solution (phonon bath). The latter leads to the broad phonon wing (PW) in the molecular spectrum. On the other hand, vibronic coupling will be expressed in the spectrum as sharp, so-called vibronic, bands,[15] although there is no sharp borderline between these two qualitatively different limiting cases. From hole burning on the FMO complex, a weak exciton−phonon coupling strength of 0.3 and a mean phonon frequency of 30 cm^{-1} were determined.[10]

As already mentioned, the pigments in a pigment−protein complex interact with the protein environment in which they are embedded. These interactions can be time-dependent. Rapid fluctuations on a time scale of less than the lifetime of the chromophore's excited state are spectroscopically reflected in the homogeneous line shape.[16] Slow changes result in static disorder, i.e., in an ensemble of a large number of molecules, the electronic transition frequencies of individual pigments will be randomly distributed around a mean value. This broadening is called inhomogeneous broadening, and the distribution is commonly referred to as the inhomogeneous distribution function (IDF). This disorder will lead to an additional broadening of the exciton spectrum, too. However, for strong (compared to the width of the IDF) exciton interactions, the exciton spectrum will be narrower than the IDF because of exchange narrowing. The width of the IDF is an important spectral parameter.

In exciton simulations, Gaussians are often superimposed on the stick spectra to give them the appearance of real spectra. One should keep in mind, however, that the experimentally observable line shape is the combined effect of the homogeneous line shape, the IDF, and exciton narrowing. For the absorption spectrum of the FMO complex, Pearlstein used Gaussians of different widths for the individual exciton states. States at energies lower than 805 nm were broadened with Gaussians of ~80 cm^{-1} full width at half-maximum (fwhm). For states higher in energy than 805 nm, Gaussians of 170 cm^{-1} fwhm were used.[8] Gülen[9] and Louwe et al.[13] both used Gaussians with a fwhm of 80 cm^{-1} for all exciton transitions. Furthermore, it is important to note that the presence of inhomogeneous broadening leads to dispersive kinetics, which are probably also important for the FMO complex of *Pc. aestuarii*.[17]

To investigate the lowest-energy absorption band of the FMO complex of *Pc. aestuarii* with an additional technique, fluorescence line-narrowing (FLN) measurements were performed. The following questions arise: What is the size of the electron−vibrational coupling in the FMO complex? What is the shape of the PW in the FMO complex? What is the width of the inhomogeneous distribution in the FMO complex? FLN has been applied earlier to pigment−protein complexes such as the B820 complex of purple bacteria,[18,19] the light-harvesting complex II of green plants,[20] and the RC of photosystem II of green plants[21] and has proven to be an excellent tool for extracting this kind of information. In combination with the temperature dependence of the absorption spectrum and computer simulations, information is obtained about the electron−vibrational coupling strength, about the PW and vibrational modes, and about the inhomogeneous broadening.

Materials and Methods

Experiments. The FMO complex of *Pc. aestuarii* was prepared as described elsewhere.[22] Samples were diluted in a buffer containing 50 mM Tris/HCl (pH = 8.3), 200 mM NaCl, and 66.6% (v/v) glycerol. The measurements were performed at 4 K in a liquid helium cryostat (Utreks). The fluorescence spectra were measured on a cooled CCD camera (Chromex ChromCam 1) via a $^1/_2$-m spectrograph (Chromex 500IS). The resolution was 0.3 nm. As the excitation source, a cw titanium-sapphire laser (Coherent 890), pumped by an argon ion laser (Coherent Innova 310), was used. The spectral bandwidth of the excitation was <1 cm^{-1}, and the excitation power was kept below 200 $\mu W/cm^2$. The emission spectra were corrected for the wavelength sensitivity of the detection system by comparing the measured emission of a standard lamp with the emission specified by the company. The absorption was measured on a home-built spectrophotometer.

Simulations. The computer simulation of the temperature dependence of electron−vibrational spectra within the linear harmonic Franck−Condon approximation is described and discussed in ref 19. We outline it briefly here.

The real observable absorption spectrum $A(\omega,T)$ at temperature T is a convolution of the homogeneous spectrum $I(\omega,T)$ with the inhomogeneous distribution function IDF(ν).

$$A(\omega,T) = I(\omega,T) \otimes \mathrm{IDF}(\nu) \tag{1}$$

(We use ω for the absolute frequency and ν for the frequency relative to the purely electronic 0−0 transition frequency Ω: $\omega = \Omega + \nu$.) Note that, within this model, the IDF is temperature-independent, and therefore, the temperature dependence is entirely due to the homogeneous spectrum. Because the IDF reflects a statistical distribution of transition frequencies, it is assumed that it corresponds to a Gaussian. The homogeneous absorption spectrum $I(\omega,T)$ can be written as

$$I(\omega,T) = \sum_{i=0}^{\infty} \frac{S(T)^i \, \mathrm{e}^{-S(T)}}{i!} l_i(\omega,T) \tag{2}$$

where i runs over the Franck−Condon progression of phonons, l_0 is the zero-phonon line (ZPL), and l_i is the convolution of l_{i-1} with the one-phonon profile $\phi(\nu,T)$. S(T) is the *effective* Huang−Rhys factor at temperature T. The usual Huang−Rhys factor S is, of course, $S(0\ \mathrm{K})$.

The one-phonon profile $\phi(\nu,T)$ is related to the phonon function $f(\nu,T)$ by

$$f(\nu,T) = S(T)\,\phi(\nu,T) \tag{3}$$

where the area of $\phi(\nu,T)$ is normalized to unity. Therefore, the effective Huang−Rhys factor at temperature T is

$$S(T) = \int_{-\infty}^{\infty} f(\nu,T)\,d\nu \tag{4}$$

The phonon function can be represented in the form

$$f(\nu,T) = [n(\nu,T) + 1]\,f_0(\nu) + n(-\nu,T)\,f_0(-\nu) \tag{5}$$

where $n(\nu,T)$ is the mean occupation number of the harmonic oscillator with frequency ν

$$n(\nu,T) = \frac{1}{\exp\left(\frac{h\nu}{kT}\right) - 1} \tag{6}$$

and $f_0(\nu)$ is the phonon density of states weighted by the electron−phonon coupling strength. The quantity $f_0(\nu)$ can be extracted numerically from the experimental spectrum of the PW $\Phi(\omega)$ at T = 0 K by[23]

$$f_0(\upsilon) = \frac{\Phi(\Omega+\nu)}{\alpha} - \frac{1}{\alpha\upsilon}\int_0^{\upsilon}\Phi(\Omega+\nu-\nu')\,\nu' f_0(\nu')\,d\nu' \tag{7}$$

where $\alpha = e^{-S(T)}$ is the Debye−Waller factor, which describes the ratio of the integrated intensities of the ZPL and the entire homogeneous absorption spectrum.

As pointed out in ref 19 this formalism can be generalized to include (intramolecular/localized) vibrational modes (vibronics) as well. The function $\phi(\nu,T)$ can then be treated as a distribution of modes, including phonons and vibrations. $\phi(\nu,T)$ will then consist of the one-phonon profile and the one-vibration profiles (i.e., spikes at the vibrational frequencies), with the intensities of the profiles being proportional to the corresponding Huang−Rhys factors. S will then be the overall Huang−Rhys factor, which is simply the sum of all of the individual Huang−Rhys factors. In the following $\phi(\nu,T)$ will be called the one-phonon-vibration profile (OPVP).

Results

Measurements. In Figure 1, the temperature dependence of the absorption of the FMO complex of *Pc. aestuarii* is shown. At room temperature, one broad absorption band can be seen. With decreasing temperature, several bands and shoulders appear in the absorption spectrum. At 4 K, (at least) three main bands can be distinguished with maxima at around 825, 814, and 805 nm. Judging from the peak positions and the shape of the absorption, the shown spectra are in good agreement with those reported for 5 and 6 K in refs 22 and 24, respectively, and for 77 and 300 K in ref 25. Whitten et al.[26] measured temperature-dependent absorption spectra of the FMO complex. However, potassium glycerophosphate was used as the cryogenic solvent in that case as opposed to glycerol in our study. Although the respective spectra in both cryogenic solvents are quite similar at low temperature (see also ref 24), the differences become larger at higher temperatures, e.g., the absorption maximum at room temperature is found around 809 nm [in a buffer containing glycerol (present data) and in a buffer without glycerol (ref 25)], whereas it is around 812 nm in glycerophosphate. Thus, the different cryogenic solvents hinder a direct comparison.

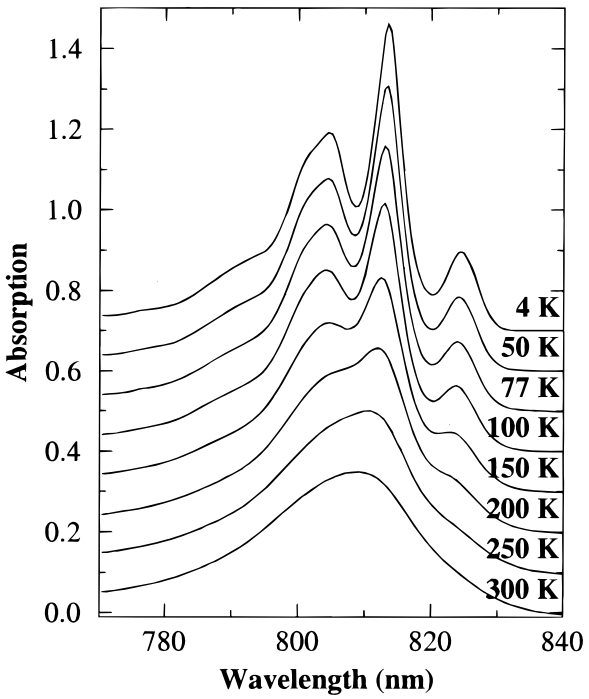

Figure 1. Absorption spectrum of the FMO complex of *Pc. aestuarii* at temperatures between 4 and 300 K. For clarity of representation, the spectra were given equidistant offsets (0.1).

In Figure 2A, the emission spectra at 4 K are shown for the complex excited in the lowest-energy absorption band around 825 nm using different excitation wavelengths. The latter are indicated in the absorption spectrum in figure 2B. The ZPL at the excitation wavelength is superimposed on scattered laser light. A separate PW can clearly be observed at all excitation wavelengths. Furthermore, several sharp bands (vibronics) can be seen on top of the PW. When the excitation wavelength is tuned to the red side of the 825 nm band, the PW sharpens, and more fine structure can be distinguished in the emission spectrum. Upon red-edge excitation, only ZPL's of the pigments are excited, and no energy transfer takes place at 4 K. However, when excitation is performed into the blue side of the band, pigments are also excited through their PW's, and furthermore, excitation energy is transferred to pigments lower in energy, from which the emission finally takes place. These effects lead to a broad and less structured emission.

Simulations. The emission at low temperature takes place from the lowest-energy state around 825 nm. Therefore, the fluorescence line-narrowing spectrum only gives information about this state, and only this absorption band is modeled. Our simulation algorithm describes the way in which the coupling of nuclear vibrations to a (localized) electronic transition contributes to the observed absorption spectrum. As the seven BChl *a* pigments in the subunit of the FMO complex are excitonically coupled, the transition, in principle, involves several pigments. However, in ref 13, it was concluded that the lowest exciton state in the FMO complex is mostly (more than 90%) localized on one single pigment. Thus, to a good approximation, we can omit the exciton description for the lowest-energy transition.

We suppose that, at 829.2 nm, we selectively excite the lowest-energy state in the FMO complex of *Pc. aestuarii* at 4 K. Within the linear harmonic Franck−Condon approximation,

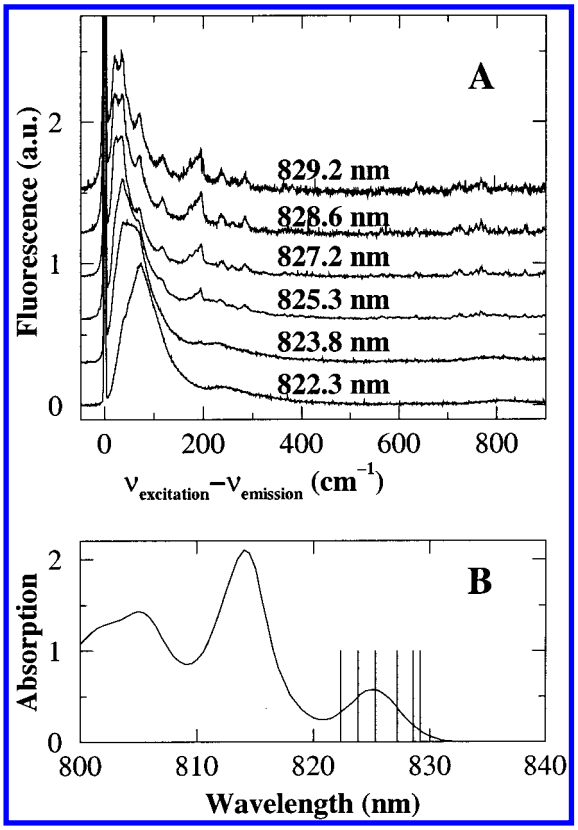

Figure 2. (A) Emission spectrum of the FMO complex of *Pc. aestuarii* at 4 K at different excitation wavelengths, which are indicated in the figure. The spectra are shown on a wavenumber scale relative to the excitation wavenumber. The spectra were normalized and given equidistant offsets. (B) Absorption spectrum of the FMO sample at 4 K used for the fluorescence measurements. The excitation wavelengths are indicated by vertical lines in the absorption spectrum.

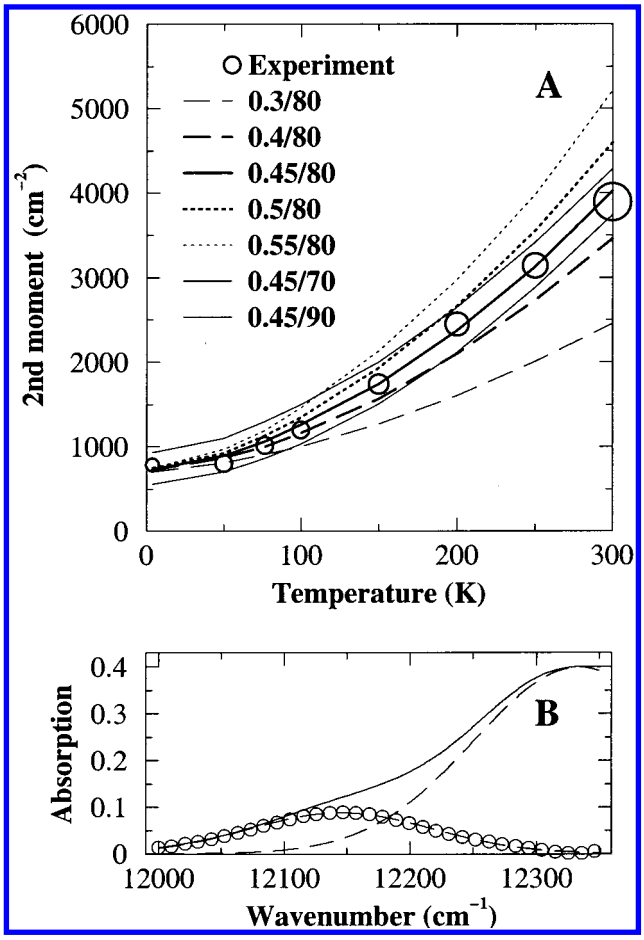

Figure 3. (A) Temperature dependence of the second moment of the lowest-energy absorption band of the FMO complex of *Pc. aestuarii*. The second moment was calculated for the low-energy side of the absorption band from the maximum to 30% of the maximum. For the experimental spectra (circles), the second moment was determined for the clean lowest-energy absorption band (see text and Figure 3B); the vertical size of the circles indicates the uncertainties in the experimental points. The simulations were performed with different choices for the Huang−Rhys factor and for the fwhm of the IDF. These are indicated in the figure. (B) Construction of the clean lowest-energy absorption band. Shown is the low-energy region of the measured absorption spectrum of *Pc. aestuarii* at 250 K on a wavenumber scale (solid line). The spectrum was fit in this spectral region with the sum of two Gaussians (dashed lines). The Gaussian at higher wavenumbers is subtracted from the measured absorption spectrum, yielding the clean low-energy absorption band (circles).

the mirror image of this emission resembles the homogeneous absorption spectrum multiplied with a factor of ν^2. The latter factor arises from the Einstein coefficients. The scattering peak was removed from the experimental spectrum, and Fourier filtering was performed. The experimental spectrum was considered here only up to ~500 cm^{-1} to prevent slight baseline effects at higher wavenumbers from entering into the integrated intensity.

Now, the absorption spectrum can be calculated at every temperature T. We choose a value for the Huang−Rhys factor and use eq 7 to extract the OPVP at T = 0 K. (It is reasonable to assume that the experimental spectrum at 4 K is very similar to the spectrum at 0 K and can therefore be used here.) With eqs 2−6, the homogeneous absorption spectrum is calculated at temperature T, taking a sharp peak ("δ function") as the ZPL. We then choose a value for the width of the IDF and calculate the observable absorption spectrum at temperature T with eq 1. Thus, with two *chosen* parameters (the Huang−Rhys factor and the width of the IDF), we can calculate the absorption spectrum at an arbitrary temperature. Note that the Huang−Rhys factor (via the Debye−Waller factor) cannot be estimated directly from the measured selectively excited emission spectrum, because the intensity of the ZPL is partially masked by scattered laser light.

The lowest-energy absorption band of the FMO complex (~825 nm) has partial overlap with the next and most intense absorption band (~814 nm). This is especially apparent at temperatures above 100 K (see Figure 1). Therefore, the experimental spectra were fit in the region from ~810 nm to ~835 nm on a wavenumber scale with the sum of two Gaussians. The Gaussian on the high-energy side was then used to construct a "clean" profile of the lowest-energy band by subtracting the former from the total absorption spectrum. This approach is illustrated for 250 K in Figure 3B.

To judge the quality of the simulations, one might directly compare the calculated and measured spectra (here the lowest-energy band). However, it proves to be much easier to compare the second moment, which characterizes mainly the width of the spectrum, of the simulated and experimental spectra.[19] If it differs for simulation and experiment, the simulations will certainly not be good. Conversely, if it is the same, one can check whether the spectra also agree. The second moment of the clean experimental lowest-energy absorption band was calculated here for the red side of the band from the position of the maximal absorption around 825 nm to the position of 30% of the maximal absorption. Only the red side of the band was used to (further) minimize the influence of the most intense absorption band (~814 nm) on the calculation of the second

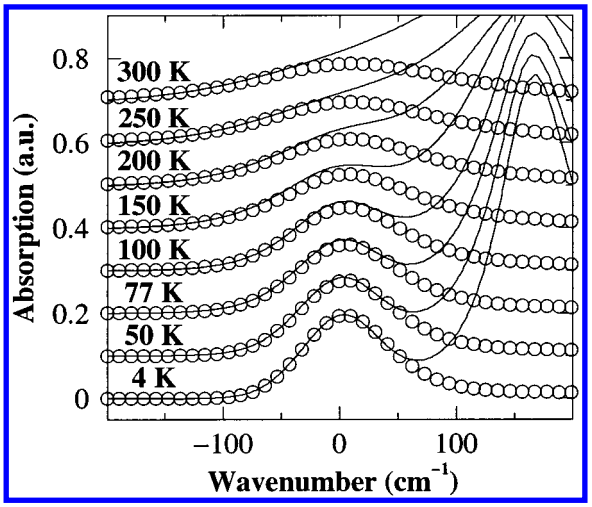

Figure 4. Comparison of the experimental absorption spectra of the FMO complex of *Pc. aestuarii* (solid lines) with the simulations (circles) at different temperatures. The spectra are shown on a relative wavenumber scale. A Huang−Rhys factor of 0.45 and a fwhm of the IDF of 80 cm^{-1} were used in the simulation. The simulation for 4 K was scaled to the corresponding experimental spectrum. It should be noted that, for the simulations at the other temperatures, the same scaling factor was used. The experimental absorption spectra were shifted on the relative wavenumber scale so that the best fit with the simulation was achieved. The spectra were given equidistant offsets.

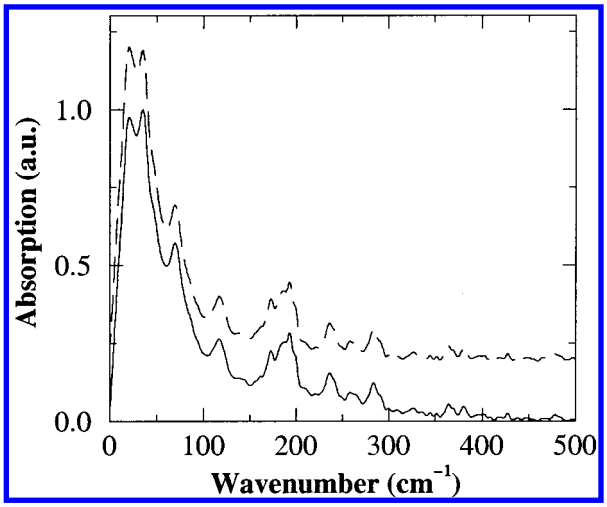

Figure 5. Spectrum of the experimental phonon-vibronic wing (solid line) and of the calculated OPVP (dashed line). The phonon-vibronic wing was constructed from the 4 K emission spectrum at 829.2 nm excitation (see Figure 2). The emission spectrum was mirror imaged, the scattering peak was removed, and the spectrum was Fourier filtered. The OPVP was calculated using eq 7 with S = 0.45. For clarity of comparison, an offset of 0.2 was added to the OPVP.

moment of the lowest-energy band. The calculation was cut off at 30% as small errors in the baseline of the measurement will contribute relatively the most to the second moment in the wings of the absorption band. For the simulated spectra, the second moment was calculated in the same way.

In Figure 3A, the experimental and simulated spectra are compared via their second moment for different choices of the Huang−Rhys factor and widths of the IDF. As shown in ref 19, the Huang−Rhys factor determines the slope of the temperature dependence of the second moment, whereas a change of the width of the IDF basically shifts the entire curve up or down. In this way, it is possible to (manually) adjust the simulation curve to fit the experimental points. It can be concluded that the simulations for S = 0.45 and fwhm$_{IDF}$ = 80 cm^{-1} fit the experiment rather well.

In Figure 4, we show the experimental absorption spectra (lowest-energy band) and the simulations for those best choices of the Huang−Rhys factor and width of the IDF. Note that the spectra are shown on a relative wavenumber scale. The experimental spectra were shifted to coincide with the simulations on the relative scale, as the model only accounts for the shape of the spectra and not for their spectral positions. Furthermore, the simulations were scaled to the experimental spectra by multiplying the calculated spectra for all temperatures with the *same* value. As already indicated by the second moment (see Figure 3), the simulations for S = 0.45 and fwhm$_{IDF}$ = 80 cm^{-1} are in good agreement with the measurements. The broadening of the spectrum with increasing temperature is well described, and also the shape of the simulated spectra closely resembles that of the measured spectra. At higher temperatures, one must realize that the absorption band around 814 nm also extends into the spectral region of the lowest-energy band. As described before, this contribution was excluded from the calculation of the second moment.

In Figure 5, the spectra of the experimental phonon-vibronic wing taken from the emission spectrum and those of the OPVP at T = 0 K extracted from it are compared. The OPVP was calculated with eq 7 for the best-fitting Huang−Rhys factor (S = 0.45). As this Huang−Rhys factor is small, the phonon-vibronic wing and the OPVP are quite close, and the main difference is that the latter is a bit narrower than the former.

The following points should be stressed. The absorption spectrum is measured and simulated. The phonon-vibronic wing (and therefore the OPVP) is obtained through an additional experiment (FLN). The power of the simulation lies in the combination of both data sets and in the fact that the full temperature dependence of the absorption is fit, thus giving reliable information about the Huang−Rhys factor and the width of the IDF. From Figure 3, it is apparent that, for example, the 4 K absorption spectrum can be fit by a range of different Huang−Rhys factors. However, by considering the *temperature dependence* of the absorption spectrum, the Huang−Rhys factor can be determined unambiguously.

Franck−Condon Factors of the Vibrational Modes. The OPVP (see Figure 5, dashed line) only contains one-phonon and one-vibration contributions. The area of the broad phonon distribution and the areas of each of the vibronic peaks are proportional to the corresponding Huang−Rhys factors S_i. For one-vibration transitions, the Franck−Condon factor FC_i is equal to $\exp(-S_i)*S_i$. Thus for $S_i < 0.1$, the Franck−Condon factor FC_i can be well approximated by S_i. Therefore, the OPVP can be used to extract the Franck−Condon factors.

In Figure 6, the OPVP (extracted from the measured phonon-vibronic wing with S = 0.45) is shown again (solid line with offset). The broad phonon distribution was accounted for by an "eye-guided smooth curve" (shown as a dotted line in Figure 6). The Franck−Condon factors of the vibrational modes are then simply proportional to the areas of the peaks, which remain after subtraction of this phonon distribution from the OPVP.

In our approach, we first determined the positions of the vibrational modes in the spectrum. Some modes cannot easily be distinguished from noise. Therefore, only those modes were considered which were consistently observed in the emission for various excitation wavelengths. The vibronic peaks were modeled as Lorentzians with a fwhm of 7.5 cm^{-1} and added to the phonon distribution. The intensities of each of the modes were manually adjusted to fit the experimental OPVP. When the area of the OPVP is scaled to the overall *S*, these intensities

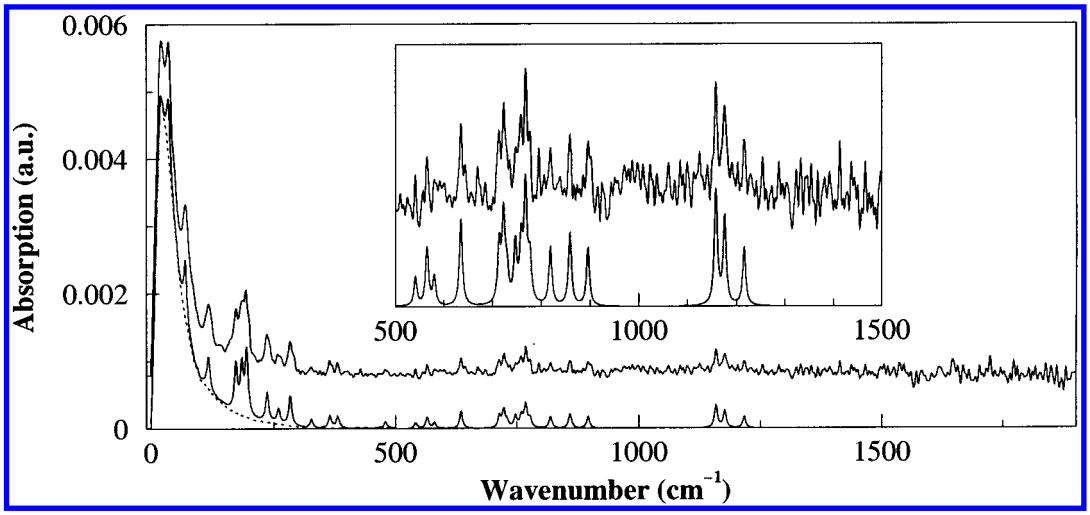

Figure 6. Shown are the OPVP, which was extracted from the measurement (solid line, arbitrary offset), the one-phonon profile (dotted line), and the calculated OPVP (solid line, no offset). The curves are scaled to the corresponding Huang−Rhys factors (see text). The inset shows a 5x magnification of the measurement-extracted OPVP (upper trace, arbitrary offset) and the calculated OPVP (lower trace) in the 500−1500 cm^{-1} region.

TABLE 1: Vibrational Frequencies Measured in the FMO Complex of *Pc. Aestuarii* and Estimated Franck−Condon (FC) Factors, Determined for $S_1 \rightarrow S_0$ Vibronic Transitions

ω (cm^{-1}) (±2)	FC factor (±50%)	ω (cm^{-1}) (±2)	FC factor (±50%)	ω (cm^{-1}) (±2)	FC factor (±50%)
36	0.01	365	0.002	747	0.002
70	0.01	381	0.002	759	0.002
117	0.0055	479	0.001	768	0.004
173	0.008	541	0.001	777	0.0015
185	0.008	565	0.002	819	0.002
195	0.011	580	0.001	859	0.0025
237	0.005	635	0.003	896	0.002
260	0.0025	714	0.002	1158	0.004
284	0.005	723	0.003	1176	0.003
327	0.0015	730	0.001	1216	0.002

will be the Franck−Condon factors of the modes, and the area of the broad phonon distribution will give the electron−phonon coupling strength. The frequencies and the Franck−Condon factors of the vibrational modes are shown in Table 1. The Huang−Rhys factor for the phonons is estimated to 0.3. The reconstructed OPVP, using the broad phonon distribution with a Huang−Rhys factor of 0.3 and the data of Table 1 for the vibrational modes, is also shown in Figure 6 (solid line without offset). It can be seen that the experimental and reconstructed OPVP are in good agreement with each other, showing that the decomposition of the spectrum into a phonon and a vibrational contribution was done properly.

Discussion and Conclusions

We showed that the temperature dependence of the lowest-energy absorption band of the FMO complex of *Pc. aestuarii* can be fit quite well. The spectral analysis was based on the linear harmonic Franck−Condon approximation and worked nicely to extract important spectroscopic parameters. The fwhm of the IDF was estimated to be 80 ± 10 cm^{-1}; strictly speaking, the IDF here is the IDF of the lowest exciton level. This width is identical to the width of the Gaussian that was used in exciton simulations to dress calculated excitonic stick spectra.[8,9,13] As can be concluded from a Monte Carlo simulation of the excitonic spectrum, the IDF of the site energies is slightly broader.[27]

The overall Huang−Rhys factor was estimated to be 0.45 ± 0.05. The electron−phonon coupling strength is 0.3. This Huang−Rhys factor in the lowest-energy absorption band agrees well with the value reported by Small and Johnson, determined from hole burning.[10] The spectral density was experimentally obtained. These results are essential for more detailed simulations of exciton dynamics in the FMO complex; for instance, the knowledge of the vibrational bands can now be included in the energy transfer calculations. Specific vibrational bands at the energy difference between two exciton states could accelerate the relaxation between those states, as pointed out by Vulto et al.[17]

Thirty vibrational frequencies can be observed in the FLN spectrum (Table 1). The strongest modes are located at 36, 70, and ∼195 cm^{-1}. From our experiment, it is, in principle, not possible to distinguish intramolecular/localized vibrations from intermolecular vibrations (phonons). As pointed out before, from a mathematical point of view, both are treated in exactly the same way. However, a possible distinction is based on the argument that a protein consists of a large number of atoms and, therefore, has a quasi-continuous distribution of nuclear modes. Thus, the phonon distribution of a protein is broad and featureless. In contrast, intramolecular/localized vibrations will be represented by sharp lines, although we cannot rule out the possibility that these vibrations are partly delocalized over the surrounding protein. This leaves us with a problem for a possible mode at 20 cm^{-1} (see Figure 6): is there a specific vibrational mode at 20 cm^{-1} or is that just the position of the maximum of the phonon distribution? This 20 cm^{-1} line is found in many different pigment−protein complexes and is generally attributed in such cases to the maximum of the phonon distribution. Therefore, we assign it in the FMO complex also as the position of the maximum of the phonon distribution rather than as a vibrational mode. The higher-frequency modes are due to intramolecular/localized vibrations of the chromophores (BChl *a*). For example, the mode at 195 cm^{-1} (see Figure 6 and Table 1) seems to be present as a relatively strong mode also in BChl *a* in glassy matrixes at 5 K in the ground state (196 cm^{-1}) and in the excited state (194 cm^{-1}).[28] However, the interaction of the protein environment with the pigments influences those modes, making it difficult to compare them, in general, with the frequencies found for BChl *a* in solution. In a hole-burning study on the B800−B850 antenna complex of *Rhodobacter sphaeroides*,[29] vibronic features were also detected. Although the reported Franck−Condon factor of BChl *a* for a mode around 750 cm^{-1} is larger than that in our study, most of the

reported features can be seen in our FLN and OPVP spectra. We mention that our FLN spectrum at 829.2 nm excitation is very similar to the Q_y-excited Raman spectrum (measured above 400 cm^{-1}) of the FMO complex.[30] Most of the modes observed in this FLN spectrum can also be seen within a couple of wavenumbers in the resonance Raman spectra following Soret or Q_x excitation[31].

The 36 cm^{-1} mode is very interesting. Such a low-frequency mode was not observed in the FLN spectra of other BChl *a* containing photosynthetic complexes. The observation of this mode allows for the possibility of another interpretation of the hole-burning data of Johnson and Small.[10] They concluded that two exciton transitions contribute to the lowest-energy absorption band in the FMO complex. Those components were at 12090 and 12130 cm^{-1}, thus having a difference in wavenumbers of 40 cm^{-1}. From our work, there is no evidence and no need to assume two (excitonic) transitions in the lowest-energy absorption band. The shape of the lowest-energy absorption band at ~825 nm can very well be explained by a single transition, for temperatures ranging from that of liquid helium up to room temperature, coupled to protein phonons and local chromophore vibrations. In the simulations by Louwe et al.,[13] there was only one excitonic transition within the lowest-energy band needed to fit various types of steady-state spectra. Our findings are in line with those results. Therefore, it is possible that the feature that was attributed by Johnson and Small to the second exciton component corresponds, in fact, to the 36 cm^{-1} mode in the data presented here.

Acknowledgment. This research was supported by The Netherlands Foundation for Scientific Research (NWO) via the Foundation for Earth and Life Sciences (ALW). M.W. received a Marie-Curie Fellowship (EC Grant ERB FMBICT 960842). M.A.P. was a guest student from Wroclaw University of Technology, supported by a Tempus grant.

Abbreviations

BChl	bacteriochlorophyll
CD	circular dichroism
FLN	fluorescence line-narrowing
FMO complex	Fenna−Matthews−Olson complex
fwhm	full width at half-maximum
IDF	inhomogeneous distribution function
LD	linear dichroism
OPVP	one-phonon-vibration profile
Pc. aestuarii	*Prosthecochloris aestuarii*
PW	phonon wing
RC	reaction center
T−S	triplet-minus-singlet
ZPL	zero-phonon line

References and Notes

(1) van Grondelle, R.; Dekker, J. P.; Gillbro, T.; Sundström, V. *Biochim. Biophys. Acta* **1994**, *1187*, 1.
(2) Sundström, V.; Pullerits, T.; van Grondelle, R. *J. Phys. Chem. B* **1999**, *103*, 2327.
(3) Blankenship, R. E.; Olson J. M.; Miller, M. In *Anoxygenic Photosynthetic Bacteria*; Blankenship, R. E., Madigan, M. T., Bauer, C. E., Eds.; Kluwer Academic Publishers: Dordrecht, The Netherlands, 1995; p 399.
(4) Fenna, R. E.; Matthews, B. W. *Nature* **1975**, *258*, 573.
(5) Tronrud, D. E.; Schmid, M. F.; Matthews, B. W. *J. Mol. Biol.* **1986**, *188*, 443.
(6) Tronrud, D. E.; Matthews, B. W. In *The Photosynthetic Reaction Center*; Deisenhofer, J., Norris, J. R., Eds.; Academic Press: San Diego, CA, 1993; Vol. I, p 13.
(7) Pearlstein, R. M.; Hemenger, R. P. *Proc. Natl. Acad. Sci. U.S.A.* **1978**, *75*, 4920.
(8) Pearlstein, R. M. *Photosynth. Res.* **1992**, *31*, 213.
(9) Gülen, D. *J. Phys. Chem.* **1996**, *100*, 17683.
(10) Johnson, S. G.; Small, G. J. *J. Phys. Chem.* **1991**, *95*, 471.
(11) Rätsep, M.; Blankenship, R. E.; Small, G. J. *J. Phys. Chem. B* **1999**, *103*, 5736.
(12) van Mourik, F.; Verwijst, R. R.; Mulder, J. M.; van Grondelle, R. *J. Phys. Chem.* **1994**, *98*, 10307.
(13) Louwe, R. J. W.; Vrieze, J.; Hoff, A. J.; Aartsma, T. J. *J. Phys. Chem. B* **1997**, *101*, 11280.
(14) Renger, Th.; May, V. *J. Phys. Chem. A* **1998**, *102*, 4381.
(15) Personov, R. I. In S*pectroscopy and Excitation Dynamics of Condensed Molecular Systems*; Agranovich, V. M., Hochstrasser, R. M., Eds.; North-Holland: Amsterdam, 1983; Chapter 10.
(16) Mukamel, S. *Principles of Nonlinear Optical Spectroscopy*; Oxford University Press: New York, 1995.
(17) Vulto, S. I. E.; de Baat, M. A.; Neerken, S.; Nowak, F. R.; van Amerongen, H.; Amesz, J.; Aartsma, T. J. *J. Phys. Chem. B* **1999**, *103*, 8153.
(18) Pullerits, T.; van Mourik, F.; Monshouwer, R.; Visschers, R. W.; van Grondelle, R. *J. Lumin.* **1994**, *58*, 168.
(19) Pullerits, T.; Monshouwer, R.; van Mourik, F.; van Grondelle, R. *Chem. Phys.* **1995**, *194*, 395.
(20) Peterman, E. J. G.; Pullerits, T.; van Grondelle, R.; van Amerongen, H. *J. Phys. Chem. B* **1997**, *101*, 4448.
(21) Peterman, E. J. G.; van Amerongen, H.; van Grondelle, R.; Dekker, J. P. *Proc. Natl. Acad. Sci. U.S.A.* **1998**, *95*, 6128.
(22) Francke, C.; Amesz, J. *J. Photosynth. Res.* **1997**, *52*, 137.
(23) Kukushkin, L. S. *Sov. Phys.−Solid State* **1965**, *7*, 38.
(24) Whitten, W. B.; Olson J. M.; Pearlstein, R. M. *Biochim. Biophys. Acta* **1980**, *591*, 203.
(25) Olson, J. M. In *The Photosynthetic Bacteria*; Clayton, R. K, Sistrom, W. R., Eds.; Plenum Press: New York, 1978; p 161.
(26) Whitten, W. B.; Nairn, J. A.; Pearlstein, R. M. *Biochim. Biophys. Acta* **1978**, *503*, 251.
(27) Wendling, M. Unpublished results.
(28) Renge, I.; Mauring, K.; Avarmaa, R. *J. Lumin.* **1987**, *37*, 207.
(29) Reddy, N. R. S.; Small, G. J.; Seibert, M.; Picorel, R. *Chem. Phys. Lett.* **1991**, *181*, 391.
(30) Robert, B. Section de Biophysique des Protéines et des Membranes, DBCM/CEA and URA 2096/CNRS, CE-Saclay, Gif-Sur-Yvette, France. Personal communication.
(31) Lutz, M.; Hoff, A. J.; Brehamet, L. *Biochim. Biophys. Acta* **1982**, *679*, 331.